Experimental validation of a discrete impact model of the rebound of a boulder on a coarse granular soil

Franck Bourrier, François Nicot, F. Darve

▶ **To cite this version:**

Franck Bourrier, François Nicot, F. Darve. Experimental validation of a discrete impact model of the rebound of a boulder on a coarse granular soil. Science et technologie des poudres et matériaux frittés 2009, May 2009, Montpellier, France. 13 p. hal-00473252

HAL Id: hal-00473252
https://hal.science/hal-00473252

Submitted on 14 Apr 2010

HAL is a multi-disciplinary open access archive for the deposit and dissemination of scientific research documents, whether they are published or not. The documents may come from teaching and research institutions in France or abroad, or from public or private research centers.

L'archive ouverte pluridisciplinaire **HAL**, est destinée au dépôt et à la diffusion de documents scientifiques de niveau recherche, publiés ou non, émanant des établissements d'enseignement et de recherche français ou étrangers, des laboratoires publics ou privés.

Experimental validation of a discrete impact model of the rebound of a boulder on a coarse granular soil

Franck Bourrier [a], François Nicot [a], and Félix Darve [b]

a Cemagref – UR ETNA - 2, rue de la Papeterie - BP 76 - 38 402 Saint Martin d'Hères Cedex – France

b L3S-R - INPG, UJF, CNRS - Domaine Universitaire - BP 53 - 38 041 Grenoble Cedex 9 - France

Graphical abstract:

The impact of a block on a coarse granular soil corresponding to rockfall events is investigated using the Discrete Element Method (DEM). The soil is considered as a noncohesive granular medium and the DEM impact model is calibrated compared to results from half-scale experiments. The effects of scale changes are also explored by comparing real-scale simulations using the DEM impact model and the half-scale experimental results. This comparison shows that using simple similitude criteria limits scale changes effects. Finally, the DEM model is used to perform a numerical analysis of the bouncing phenomenon. Different impacting particle and medium characteristics are considered. An impacting particle bouncing occurrence diagram is defined for various impacting particle radius R_b^*/R_m, sample heights H^*/R_m, and incident kinematic parameters. The bouncing occurrence diagram brings out three impact regimes. For a small impacting particle ($R_b^*/R_m < R_{crit}^*/R_m$), the impact is mainly determined by the first interaction between the impacting particle and the soil, whereas for an intermediate-sized impacting particle ($R_{crit}^*/R_m \leq R_b^*/R_m < R_{min}^*/R_m$), the compression wave propagation through the sample is the leading phenomenon. For large impacting particles ($R_b^*/R_m \geq R_{min}^*/R_m$), bouncing is associated with the formation of a compact layer below the impacting particle.

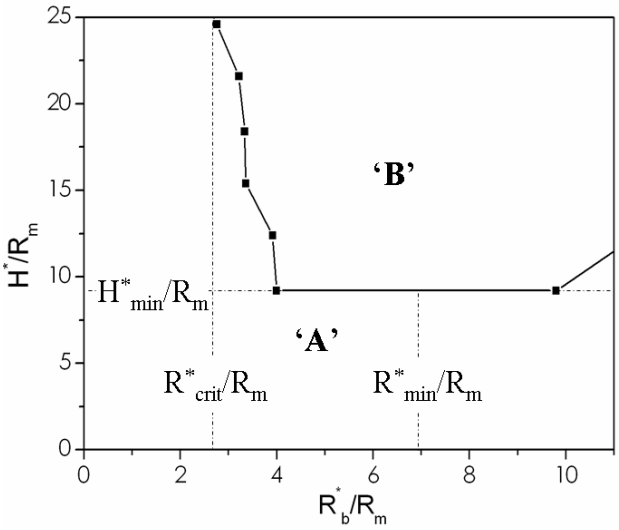

Bouncing occurrence diagram.

Keywords: Impact, Discrete Element Method, Experiments, Rebound, Wave propagation.

1. Introduction

Rockfall is a major risk in mountainous zones. Designing defense structures against rockfall is a difficult task in which the prediction of the trajectories of the falling boulders is essential. Trajectory analyses are therefore performed to inform practitioners on the potential trajectories of the falling boulder within the area to be protected. In the field of falling rocks trajectory simulations, many scientific problems related to modelling the bouncing phase remain to be solved.

The purpose of this paper is to investigate the physical mechanisms that govern the bouncing of an impacting particle onto a granular assembly. Numerical simulations using discrete modelling of the soil are presented. The first step of the procedure is numerically modeling, in a 2D context, a single interaction between the falling boulder and the scree using the discrete element method (DEM). The validity of the DEM simulation procedure is evaluated by comparing results from half-scale experiments with simulations using the DEM impact model. The effects of scale changes are also explored in order to evaluate the relevance of using the DEM impact model, which is calibrated from half-scale experiments,

for real-scale studies. Finally, the analysis of the impacting particle bouncing occurrence is performed in order to define different impact types associated with different physical processes.

2. Discrete Element Method impact model

Assuming that rocks composing a coarse soil can be considered as rigid locally deformable two-dimensional bodies, the software Particle Flow Code 2D [1] based on the Discrete Element Method [2] is used. In the Discrete Element Method, contact forces are applied to particles in contact. In this study, the contact forces acting between particles are calculated using the Hertz-Mindlin model [3].

The mean radius of soil particles is $R_m = 0.3\ m$. Given that natural scree are polydisperse granular assemblies, the ratio between the mass of the soil's smaller rocks and larger rocks is set at 10. Additional details on the soil properties can be found in [4].

In the case of the impact on a coarse granular soil, boulder and soil particle sizes are nearly the same. Boulder radius R_b therefore varies from R_m to $5R_m$. Sample properties are defined following the procedure used in [4]. The influence of particle shape is also explored by defining two different soil samples composed of either spherical particles or elongated particles modeled by indivisible assemblies of spherical particles called clump particles, which allow modeling the shape of rocks in a realistic way [4].

The soil sample is generated from distinct particles subjected to gravitational forces only. Gravitational forces are applied to all particles and a calculation procedure is run until the total kinetic energy of the system lowers a set value. The porosity of the sample is controlled by the value of the local friction angle during the generation process. After sample generation, the local friction angle is set at $\varphi = 30°$ and sample depth is set at $12R_m$.

Once the soil sample is generated, impact simulations can be held for varying impact points and incident kinematic parameters. The location of each impact point is precisely defined. In addition, incident kinematic conditions are fully characterized by the magnitude of the incident velocity V^{in}, the incident angle α^{in} and the incident rotational velocity ω^{in} (Fig. 1). These parameters are directly related to the normal V_y^{in} and tangential V_x^{in} velocity components by the relations:

$$V_x^{in} = V^{in} \sin(\alpha^{in}) \qquad (1)$$

$$V_y^{in} = -V^{in} \cos(\alpha^{in}) \qquad (2)$$

Finally, reflected velocities are collected when the normal component of the boulder velocity reaches its maximum, which corresponds to the last contact between the soil and the boulder.

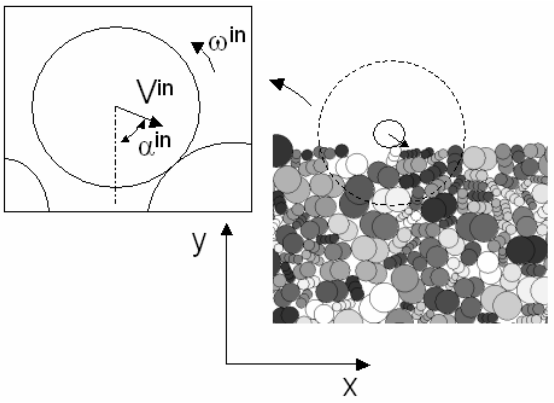

Fig. 1. Incident kinematic conditions.

3. DEM impact model validation

3.1. Half-scale experiments

The validity of the DEM impact model is evaluated by comparing predictions using this model with results from half-scale experiments [5]. The experiments (Fig. 2) consist of the impact of a rock, whose equivalent diameter is 6.8 *cm*, on a coarse soil composed of limestone rocks having approximately the same size as the impacting rock. The impacting rock is a quasi-spherical granite projectile that limits projectile breakage during impact and facilitates the calculation of the velocity of the impacting rock. A specific projectile dropping device was designed and calibrated in order to control the magnitude and the direction of the incident velocity of the projectile. The incident velocity of the projectile is 6 m/s and the incident angle can reach values from 0° to 75°. The component of the incident velocity along the *z* axis (Fig. 2) and the incident rotational velocity are always nil.

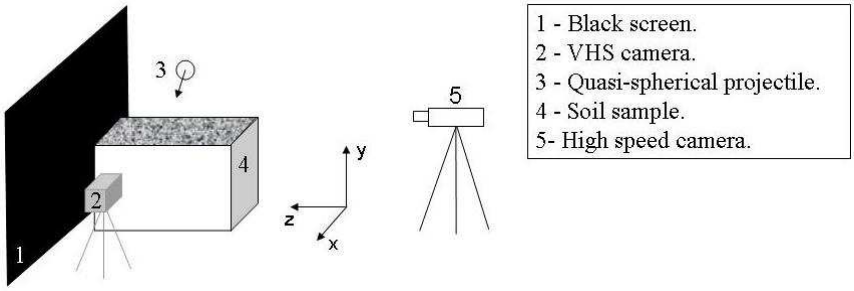

Fig. 2. Experimental set-up.

The impact experiments were filmed in the *xy* plane using a high-speed camera and in the *yz* plane using a VHS camera (Fig. 2). The analysis of VHS films showed that the reflected velocity of the boulder along the *z* axis was negligible toward the other components of the reflected velocity. Image processing of the films from the high-speed camera therefore allowed the calculation of the normal and tangential components of the reflected velocity of the boulder. More than 100 impact experiments were conducted for varying incidence angles. The values of the incidence angle varied from 0° to 75° and the same number of impact experiments were conducted for each incidence angle value explored (0°, 15°, 30°, 45°, 60°, 75°).

3.2. Comparison between experimental and simulation results

In order to remove the effects of scale changes, the DEM model described in section 2 was first adapted. The characteristics of the numerical model were therefore defined to match the properties of the experimental soil sample and the experimental incident conditions. In particular, the impacting sphere radius was set at the same value as the equivalent radius of the granite rock used in the experiments. Additionally, clump particles were used in the DEM model. The size of the particles of the numerical sample were determined in order to come close to the experimental grading curve and the distribution of the size ratio, defined as the ratio of the particles' length to the particles' width, of the rocks composing the experimental soil sample. One can also note that the Hertz–Mindlin contact law is still used and that

the values of the mechanical properties of the particles are similar to those defined in section 2 (G = 40 GPa, ν = 0.25, φ = 30°, and ρ = 2650 kg/m^3).

The porosity of the numerical soil sample is considered a calibration parameter because no simple relation exists between the 3D porosity of the experimental soil sample and the 2D porosity of the numerical soil sample. The numerical simulations were therefore performed using several numerical soil samples with different 2D porosities.

The simulation results obtained were compared with the experimental results. Both the cumulative distribution functions of the tangential V_x^{re} and normal V_y^{re} to soil surface components of the reflected velocity were compared.

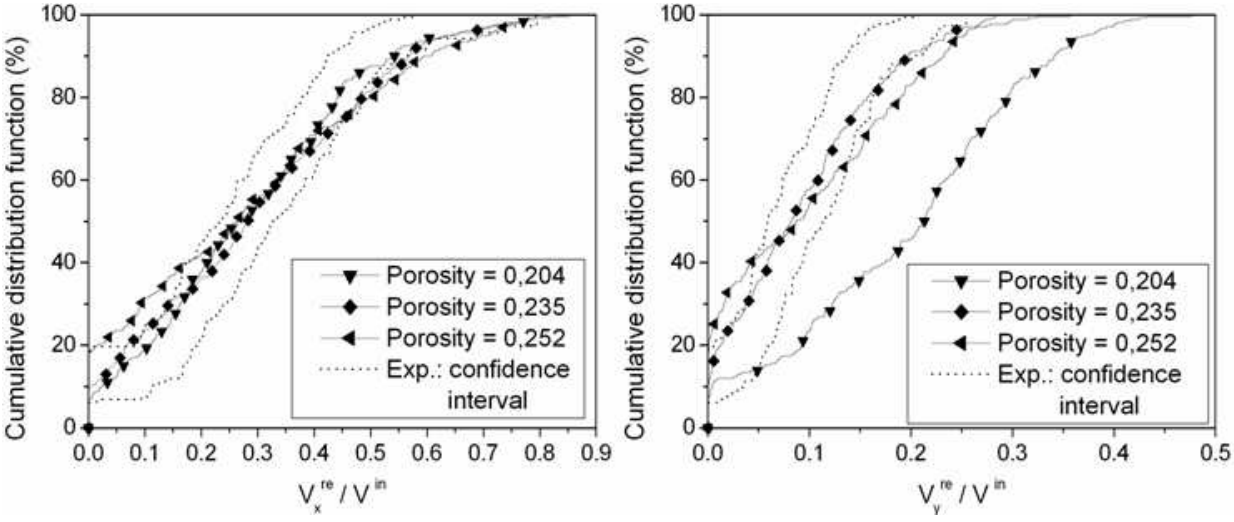

Fig. 3. Cumulative distribution functions of the tangential V_x^{re} and normal V_y^{re} components of the reflected velocity obtained in the experiments and in the simulations. Simulation results of impacts on different soil samples of varying porosity are compared with the experimental results.

The results highlight a fair accordance between the cumulative distribution functions of the reflected velocity components in the simulations and the experiments (Fig. 3). The tangential component V_x^{re} of the velocity was predicted particularly well using the DEM impact model because, whatever the porosity of the numerical soil sample, the cumulative distribution function of the simulation results was contained

within the confidence interval associated with the experimental results (Fig. 3). In addition, the porosity of the numerical soil sample did not change the results for the tangential component V_x^{re}. On the contrary, the values of the normal component V_y^{re} strongly depended on the porosity of the numerical soil sample (Fig. 3). However, one can find a value of the porosity of the numerical soil sample that allows satisfactorily approaching the experimental results for both components V_x^{re} and V_y^{re}. This proves that the DEM properly models the impact of a rock on a coarse soil for a reduced number of calibration parameters: the porosity of the soil sample is the only simulation parameter to be calibrated.

3.3. Scale changes effects

The DEM impact model is also used to compare numerical simulations at real-scale, corresponding to rockfall events conditions, to experimental results to evaluate the accuracy of using the DEM impact model, which is calibrated from half-scale experiments, for real-scale studies. The porosity of the numerical soil sample is set at 0.235 which corresponds to the value providing the best accordance with the experimental results in the previous section. All sizes in the model (overall sizes of the sample, impacting particle and soil particles sizes) are defined by a homothetic transformation of experimental parameters. The homothetic transformation ratio is defined so that the impacting particle radius in the DEM model R_b is equal to 0.4 m. In addition, in the simulations, the incident velocity V^{in} values are chosen so that the ratio between the incident kinetic energy and the gravitational energy corresponding to a particle falling down from a height equal to its diameter is conserved in the experiments and in the simulations. This similitude criterion leads to keep the same values of the Froude number in the simulations and in the experiments. Froude number *Fr* is defined as follows:

$$Fr = \frac{V^{in}}{\sqrt{2gR_b}} \qquad (3)$$

This simple similitude criterion [6, 7] does not integrate all similitude rules given the complexity of the mechanisms occurring during the impact. In particular, it does not allow keeping the value of the ratio between the maximal stress applied on soil particles and the rock's yield stress.

Simulations are performed for different values of *Fr* near the experimental value *Fr* = 7.5. Simulations for Froude number values of 3.5, 5, and 7.5 (i .e. for incident velocities equal to, respectively, 10 m/s, 15 m/s, and 20 m/s) are conducted. Other incident conditions are the same as in the experiments: ω^{in}=0 rad/s, $0° \leq \alpha^{in} \leq 75°$.

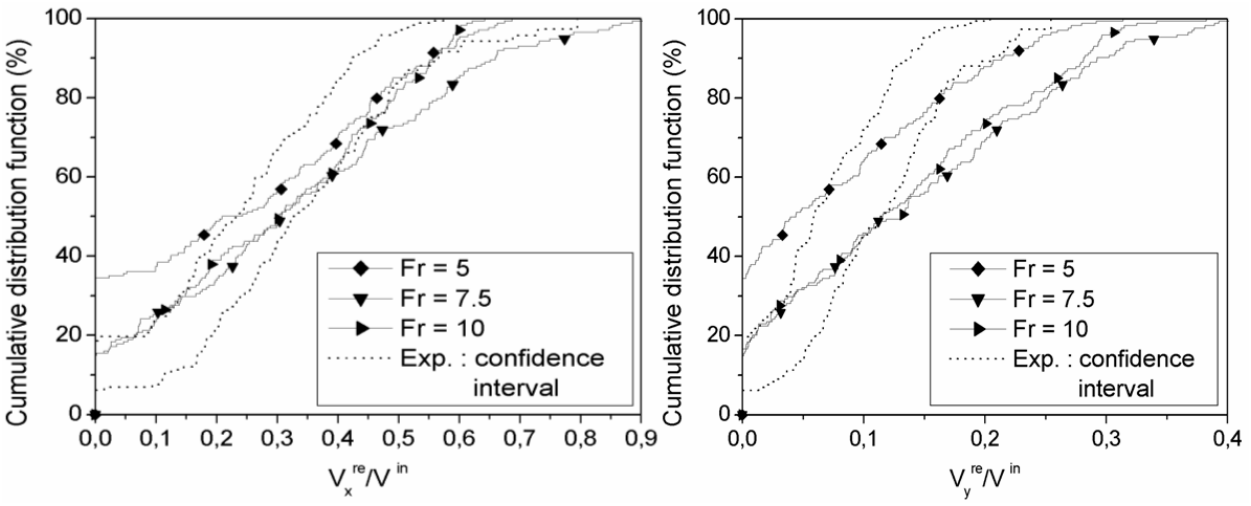

Fig. 4. Comparison between the cumulative distribution functions of the tangential V_x^{re} and normal V_y^{re} to soil surface components of the reflected velocity obtained in the experiments and in "real-scale" simulations. Several simulation results corresponding to different Froude numbers (i.e. incident velocities) are compared with the experimental results.

The purpose of the comparison is to evaluate the relevance of using a similitude criterion based a homothetic transformation of all sizes combined with a conservation of Froude number.

Whatever the incident velocity, the simulations predict less accurately the experiments than those performed at the same scale as the experiments. Although the tangential component of the velocity is well predicted, the simulation results for the normal component are in poorer agreement with the experimental result. However, similar varying ranges are obtained for all velocity components which tend to prove that simple similitude rules are sufficient to obtain a minimal predictability of the simulations at real-scale.

The differences observed are mainly due to the fact that the similitude criterion used does not account for the complexity of the mechanisms occurring during the impact. In addition, these differences could be

explained by the fact that the assumptions regarding 3D effects, grading curves, and angularity of the particles do not act in the same proportions in half-scale and real-scale simulations.

4. Physical analysis of the rebound using the DEM impact model

4.1. Bouncing occurrence diagram

Several impact simulations are conducted for varying impact points and incident kinematic parameters using the DEM impact model described in section 2. The bouncing is studied for varying impacting particle radius R_b ($0.3R_m < R_b < 15\ R_m$), sample heights H ($5R_m < H < 25\ R_m$) and impacting particle incident angle α^{in} ($0° < \alpha^{in} < 75°$) and velocity V^{in} (5 m/s < V^{in} < 40 m/s). Preliminary numerical investigations have shown that, for each parameter set explored, a minimum of *N=100* impact points must be used so that the simulations are statistically representative [4].

A global definition of a bouncing occurrence is established in order to free from local effects. For a given set of parameters $(H,R_b,V^{in},\alpha^{in})$, the global bouncing criterion is defined as the percentage of local bouncing occurrences for varying impact points. If the percentage of bouncing occurrences is higher than a threshold value *S=75%*, the parameters tested are associated with bouncing occurrence. Otherwise, they are associated with stopping on the soil.

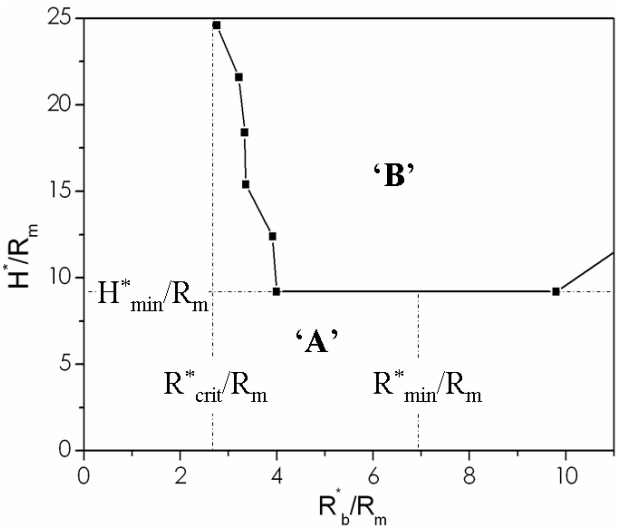

Fig. 5. Bouncing occurrence diagram for fixed incident kinematic conditions.

For fixed incident kinematic conditions (V^{in*},α^{in*}), the curve delimiting impacting particle bouncing and stopping occurrence (Fig. 5) is defined in the two-dimensional space (R_b,H). Impacting particle bouncing is associated with the domain *'A'* below the curve and particle stopping on the soil is associated with the domain *'B'* (Fig. 5). The curve delimiting the *'A'* and *'B'* domains passes through a minimum value for (R^*_{min}, H^*_{min}), and a vertical asymptote seems to exist for $R^*_b/R_m \approx R^*_{crit}/R_m$.

Three impact regimes can be defined depending on the impacting particle size. The first impact regime corresponds to $R_b < R^*_{crit}$. In the first impact regime, the impacting particle bounces for any sample height. The second impact regime is delimited by an impacting particle radius range within the limits $R^*_{crit} < R_b < R^*_{min}$. In the second regime, the curve delimiting the *'A'* domain and the *'B'* domain decreases as R^*_b value increases. The third impact regime has an impacting particle radius larger than R^*_{min}. Contrary to what is observed for the second regime, the delimiting curve is characterized by an increase in the H^* value as the R^*_b value increases.

4.2. Physical processes during impact

The impact of the particle on the soil is composed of successive contact interactions between the impacting particle and soil particles. The first contact interaction is associated with a partial energy exchange from the impacting particle to the soil sample. The impacting particle's incident energy is substantially reduced during this phase. In addition, depending on the boulder radius, the normal to soil surface component of the boulder velocity inverses or not during the first phase. If this component inverses, bouncing directly occurs during the first energy exchange. This corresponds to the first impact regime in which bouncing directly occurs because of the small size of the impacting particle compared to the mean size of soil particles [4].

On the contrary, for larger boulder sizes, bouncing does not occur during the first phase and the impacting particle continues penetrating inside the soil sample. The initial energy transfer gives rise to a sudden increase in the total energy of the soil which brings the particles of the central crown out of equilibrium,

inducing their movement. The displacement of the previous particles also brings the particles of the second crown out of equilibrium leading to a kinetic energy peak on the second concentric crown [4]. The energy peaks are time-delayed from one crown to the adjacent one. This phenomenon has already been described on a one-dimensional column of beads [8,9,10] and two-dimensional media [11]. This is relevant for compression wave propagation.

In the second impact regime, the total incident kinetic energy is totally transferred to the soil by successive interactions between the impacting particle and the soil particle. Bouncing is therefore only possible if energy is transferred again from the soil particles to the impacting particle. As no significant penetration of the impacting particle inside the soil occurs, the cause of the bouncing is a second energy exchange from the soil after the compression wave round trip inside the sample [4]. This second energy exchange occurs if the incident kinetic energy is not totally dissipated during the wave's round trip which depends on sample height and explains why bouncing is not possible whatever sample height.

In the third impact regime, impacting particle penetration becomes appreciable. Since impacting particle radius is large, the dissipation processes inside the sample are not sufficient to dissipate the incident kinetic energy. Substantial impacting particle penetration occurs because the kinetic energy that is not dissipated leads to substantially deforming the sample. Thus, bouncing occurs when the compacity of the bottom layer is high enough to ensure the growth of stable force chains in which normal forces can develop and contribute to the bouncing of the impacting particle. If bouncing occurs, the height of the bottom layer between the bottom wall and the impacting particle is therefore equal to a critical value, which is a function of the sample height [4].

5. Conclusions

In this paper, a numerical model of the impact of a boulder on a coarse granular material was first developed using the DEM. The DEM impact model was first evaluated and calibrated using results from half-scale experiments. The effects of scale changes were also explored by comparing half-scale experimental results to real-scale simulations corresponding to rockfall eventsconditions. The parameters

of the real-scale simulations were determined by using a simple similitude criterion based on keeping the value of the Froude number and performing a homothetic transformation of all geometric parameters values. The comparison shows that, although the real-scale simulations do not fully allow predicting the experiments, the main characteristics of the experimental results are traduced. In particular, the ranges of velocities are well predicted. This proves that using simple similitude criteria is sufficient to globally account for scale changes effects.

The numerical investigations using the DEM model presented in this paper also provide an overview of the phenomena governing the impact on a coarse granular soil. Bouncing is explored for all local configurations by exploring several impact points and defining a global bouncing existence criterion.

This procedure provides a diagram delimiting impacting particle bouncing and stopping depending on the sample height and impacting particle size for given incident kinematic conditions. This diagram illustrates the existence of three impact regimes depending on impacting particle size. The first impact regime corresponds to small boulder size. In this case, the impact process is mainly governed by the initial interaction between the impacting particle and the soil. The second impact regime is associated with intermediate impacting particle radii. For the second regime, impacting particle bouncing is attributable to a second energy supply from the soil after the compression wave's round trip through the sample if the impacting particle's incident energy is not fully dissipated through frictional processes during the round trip. The third impact regime corresponds to large impacting particle radii. The impact here leads to substantial penetrations within the sample and bouncing is the result of the interaction of the impacting particle with a thin compacted layer. Although the results obtained clearly show that three impact regimes exist in the context of the simulations performed, whether these regimes exist for real rockfall events is still to be proved. However, the results obtained provide a basis for further simulations.

References

1. Itasca Consulting Group, PFC2D User's manual, Minneapolis: Itasca, 1999.

2. P.A. Cundall and O.D.L. Strack, A discrete numerical model for granular assemblies, *Geotechnique* **29**, 47-65 (1979).

3. R.D. Mindlin and H. Deresiewicz, Elastic spheres in contact under varying oblique forces, *Journal of Applied Mechanics* **20**, 327-344 (1953).

4. F. Bourrier and F. Nicot and F. Darve, Physical processes within a 2D granular layer during an impact, *Granular Matter* **10**(6), 415-437 (2008).

5. F. Bourrier and N. Eckert and H. Bellot and A. Heymann and F. Nicot and F. Darve, "Numerical modelling of physical processes involved during the impact of a rock on a coarse soil" in *Advances in Geomaterials and Structures*, edited by F. Darve et al.. AGS'08 Proceedings, Collection S.T., Hammamet, Tunisia, 2008, pp. 501-506.

6. F. Rioual and A. Valance and D. Bideau, Experimental study of the collision process of a grain on a two-dimensional granular bed, *Physical Review E* **62**, 2450-2459 (2000).

7. D. Beladjine and M. Ammi and L. Oger, L. and A. Valance, A, Collision process between an incident bead and a three-dimensional granular packing, *Physical Review E* **75**, 1-12 (2007).

8. C.S. Campbell, A problem related to the stability of force chains, *Granular Matter* **5**, 129-134 (2003).

9. C. Coste and E. Falcon and S. Fauve, Solitary waves in a chain of beads under Hertz contact, *Physical Review E* **56**(5), 6104-6117 (1997).

10. S. Job and F. Melo and A. Sokolow and S. Sen, Solitary wave trains in granular chains: experiments, theory and simulations, *Granular Matter* **10**, 13-20 (2007).

11. S.R. Hostler and C.E. Brennen, Pressure wave propagation in granular bed, *Physical review E* **72**(3), 1-13 (2005).